Supporting Information for

Base-controlled Mechanistic Divergence between Iron(IV)-Oxo and Iron(III)-Hydroperoxo in the H_2O_2 Activation by a Nonheme Iron(II) Complex.

Antoine Bohn, Clémence Chinaux-Chaix, Khaled Cheaib, Régis Guillot, Christian Herrero, Katell Sénéchal-David, Jean-Noël Rebilly, Frédéric Banse

Experimental Section.

All moisture and oxygen sensitive compounds were prepared using standard high vacuum line, Schlenk and cannula techniques. All reagents were purchased from Aldrich or Acros and used as received unless noted otherwise. Acetonitrile solvent was purified by distillation, under argon, over CaH_2.

$[Fe^{II}(L_5^{2})](MeCN)](PF_6)_2$ (1) was prepared by reacting $[Fe^{II}Cl(L_5^{2})](PF_6)$[1] (635 mg, 1.09 mmol) with 1.1 equiv. $AgPF_6$ in MeCN at RT. The initial yellow solution became red and turbid upon AgCl precipitation. The mixture was stirred for 2 hours, concentrated by evaporation of the solvent under low pressure and placed at -20°C overnight. The white precipitate was then filtrated off and the resulting solution was placed at -20°C overnight. Finally, the remaining solid was removed by using a syringe with a 0.45 μm teflon filter. Addition of Et_2O yielded $[Fe^{II}(L_5^{2})(MeCN)](PF_6)_2$ as a red solid (500 mg, 86%). Single crystals were obtained by layering an acetonitrile solution of the complex with Et_2O.

$[Fe^{IV}O(L_5^{2})]^{2+}$ was obtained following the procedure reported by Thibon et al.[2] Reaction of $[Fe^{II}(MeCN)(L_5^{2})]^{2+}$ (1.6 mM) with excess solid PhIO in MeCN at RT was stirred until decoloration of the intense red orange color of the Fe^{II} precursor. The residual PhIO was then removed by filtration to leave a clear green solution.

UV-visible absorption spectrophotometry was performed with a Varian Cary 60 spectrophotometer equipped with a Hellma immersion probe (1 cm optical path length) and fiber-optic cable. Low temperature was maintained using a Thermo Haake CT90L cryostat.

Stopped Flow absorption spectrophotometry was performed at 20°C on a BioLogic SFM-4000 coupled to a J&M Tidas diode array spectrometer. Final concentration in Fe was 2 mM.

X-band EPR X-band EPR spectra were recorded at 90 K on a Bruker ELEXSYS 500 spectrometer equipped with a Bruker ER 4116DM X band resonator, an Oxford Instrument continuous flow ESR 900 cryostat, and an Oxford ITC 503 temperature control system.

X-ray diffraction data for $[Fe^{II}(L_5^{2})](MeCN)](PF_6)_2$ (**1**) were collected by using a Bruker AXS Kappa ApexII Diffractometer with 0.71073 Å Mo-Kα radiation. Crystal was mounted on a CryoLoop (Hampton Research) with Paratone-N (Hampton Research) as cryoprotectant and then flashfrozen in a nitrogen-gas stream at 100 K. For compound **1**, the temperature of the crystal was maintained at the selected value by means of a 700 series Cryostream cooling device to within an accuracy of ±1K. The data were corrected for Lorentz polarization, and absorption effects. The structures were solved by direct methods using SHELXS-97[3] and refined against F^2 by full-matrix least-squares techniques using SHELXL-2018[4]with anisotropic displacement parameters for all non-hydrogen atoms. Hydrogen atoms were located on a difference Fourier map and introduced into the calculations as a riding model with isotropic thermal parameters. All calculations were performed by using the Crystal Structure crystallographic software package WINGX.[5] The crystal data collection and refinement parameters are given in Table S1.

CCDC 1944504 contains the supplementary crystallographic data for this paper. These data can be obtained free of charge from the Cambridge Crystallographic Data Centre via http://www.ccdc.cam.ac.uk/Community/Requestastructure.

Table S1. Crystallographic data and structure refinement details.

Compound	**$[Fe^{II}(L_5^2)(CH_3CN)](PF_6)_2$ (1(PF_6)$_2$)**
CCDC	1944504
Empirical Formula	$C_{23}H_{28}FeN_6, 2(F_6P)$
M_r	734.30
Crystal size, mm^3	0.21 x 0.10 x 0.09
Crystal system	monoclinic
Space group	$P\ 2_1/n$
a, Å	16.4343(4)
b, Å	20.4024(5)
c, Å	17.2272(5)
α, °	90
β, °	17.2272(5)
γ, °	90
Cell volume, Å^3	5773.6(3)
Z ; Z’	8 ; 2
T, K	100(1)
Radiation type ; wavelength Å	Mo-Kα ; 0.71073
F_{000}	2976
μ, mm^{-1}	0.738
θ range, °	1.547 - 30.594
Reflection collected	104 511
Reflections unique	17 680
R_{int}	0.0680
GOF	1.024
Refl. obs. ($I>2\sigma(I)$)	12 203
Parameters	840
wR_2 (all data)	0.1032
R value ($I>2\sigma(I)$)	0.0419
Largest diff. peak and hole (e-.Å^{-3})	0.688 ; -0.532

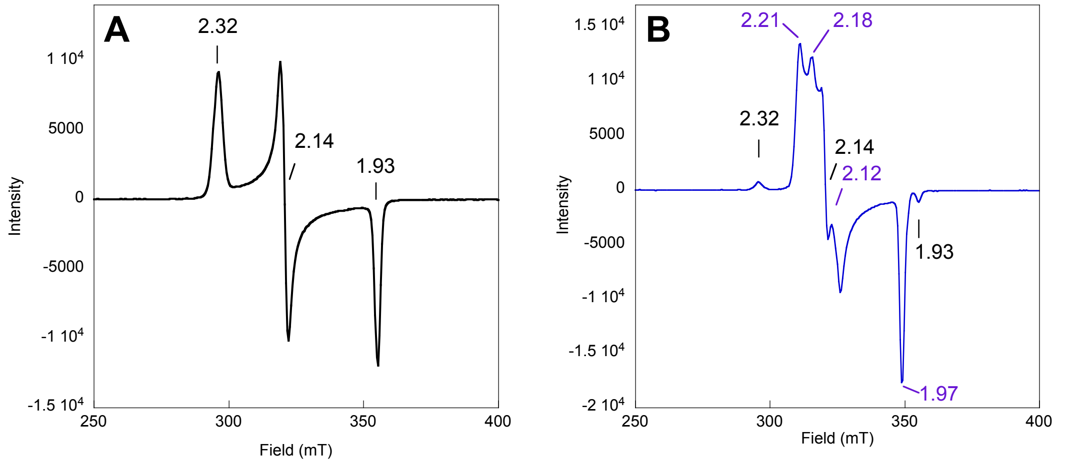

Figure S1. (**A**) X-band EPR at 90 K of $[Fe^{III}(OR)(L_5^{2})]^{2+}$ (R = H, Me) obtained from $[Fe^{II}(L_5^{2})(MeCN)]^{2+}$ (**1**, 2 mM) and 1 equiv. H_2O_2 in CH_3OH at 20°C. (**B**) X-band EPR at 90 K of the sample obtained from $[Fe^{II}(L_5^{2})(MeCN)]^{2+}$ (**1**, 2 mM) and 50 equiv. H_2O_2 in CH_3OH at 20°C. The characteristic resonances of $[Fe^{III}(OOH)(L_5^{2})]^{2+}$ are indicated by purple labels, those related to $[Fe^{III}(OR)(L_5^{2})]^{2+}$ are indicated by black labels. Microwave frequency 9.6 GHz, microwave power 1 mW, modulation amplitude 8 G, gain 50 dB.

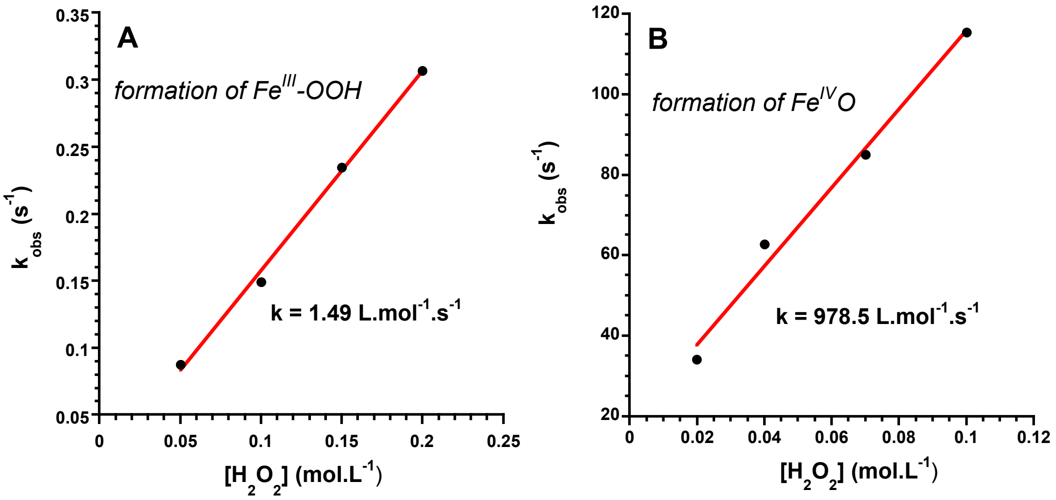

Figure S2. Plot of the observed rate constant as a function of the concentration of hydrogen peroxide for the formation of $[Fe^{III}(OOH)(L_5^{2})]^{2+}$ (generated from **1**, 2 mM, and H_2O_2) (**A**) and for the formation of $[Fe^{IV}O(L_5^{2})]^{2+}$ (generated from **1**, 2 mM, and H_2O_2 in the presence of 0.7 NEt_3) (**B**).

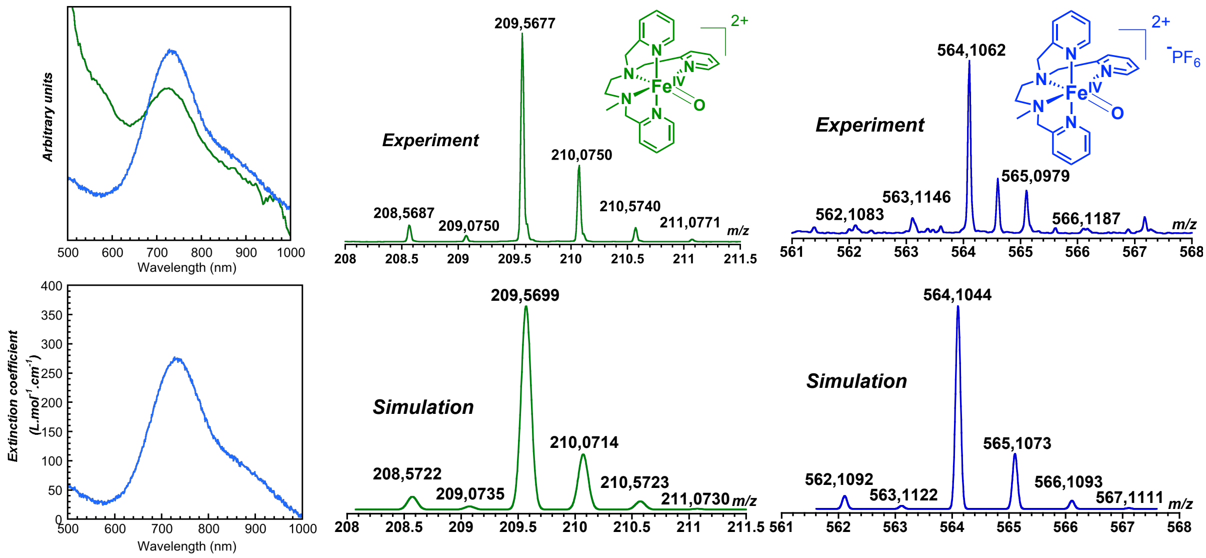

Figure S3. Visible absorption (left) and experimental and theoretical ESI-MS features (right) of $[Fe^{IV}O(L_5^2)]^{2+}$ obtained from $[Fe^{II}(L_5^2)(MeCN)]^{2+}$ (**1**) and PhIO in CH_3CN. The top left panel overlays the visible absorption spectrum of $[Fe^{IV}O(L_5^2)]^{2+}$ obtained from **1** and PhIO (blue trace) with the one obtained from the reaction of **1** with 50 H_2O_2 and 0.7 NEt_3 (green trace) corresponding to the bold green trace in Figure 3 of the main text.

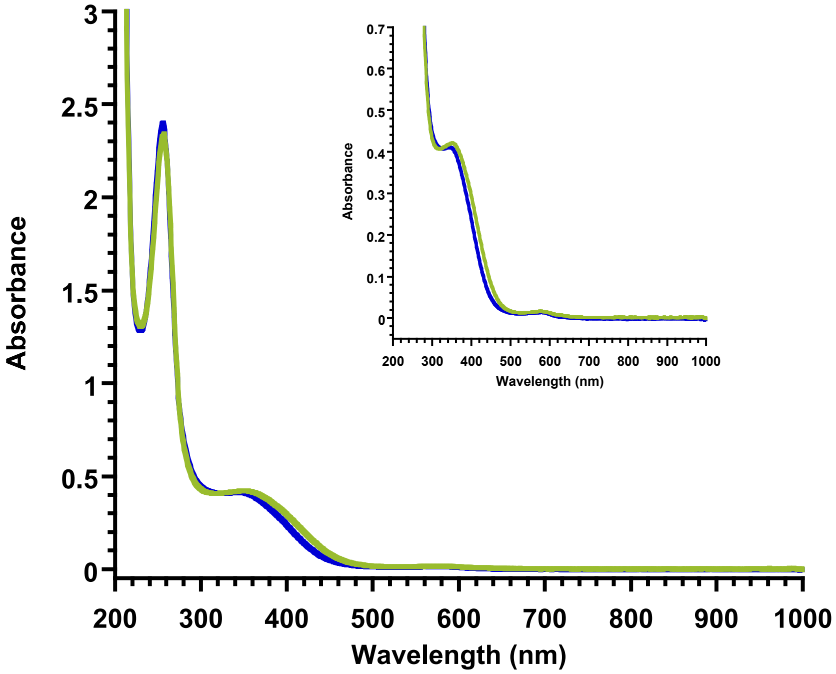

Figure S4. UV-visible absorption spectrum of $[Fe^{II}(L_5^2)(MeCN)]^{2+}$ (**1**) in CH_3OH in the absence (blue) or in the presence (green) of 0.7 eq. NEt_3.

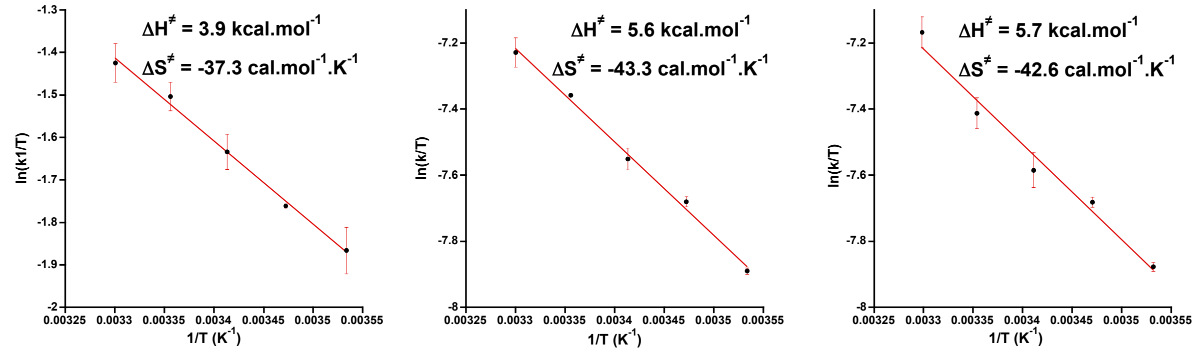

Figure S5. Eyring plots for the formation of $[Fe^{IV}O(L_5^2)]^{2+}$ (left) and $[Fe^{III}(OOH)(L_5^2)]^{2+}$ (middle) in the reaction of **1** (2 mM) with 50 equiv. H_2O_2 in the presence of 0.7 equiv. NEt_3 in CH_3OH. (Right) Eyring plot for the formation of $[Fe^{III}(OOH)(L_5^2)]^{2+}$ in the reaction of **1** (2 mM) with 50 equiv. H_2O_2 in CH_3OH in the absence of NEt_3.

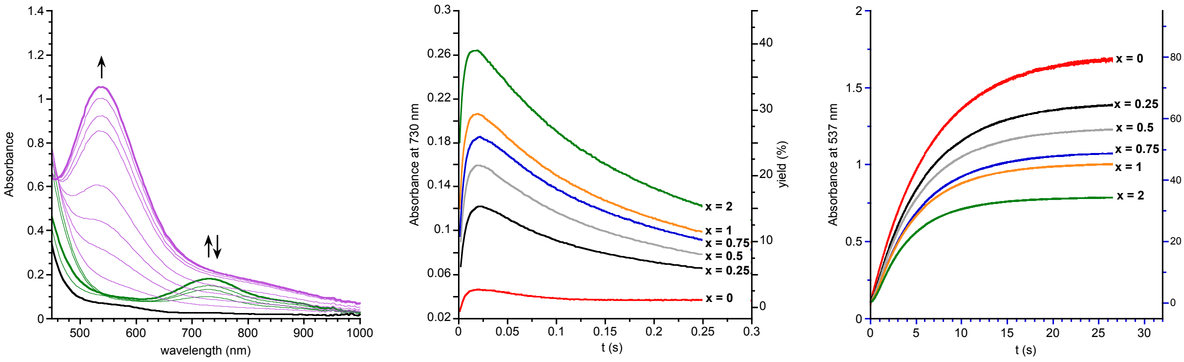

Figure S6. Time resolved UV-Vis spectra of **1** (2 mM) before (black) and after addition of 50 equiv. H_2O_2 in the presence of 0.75 equiv. 2,6-lutidine in CH_3OH at 20°C. The green traces were recorded 12 ms, 24 ms (bold trace), 108 ms, and 204 ms, respectively, after mixing the reactants. The purple traces were obtained after 804 ms, 1.6 s, 2.5 s, 4 s, 8 s, 10 s, 14 s and 20 s; (left). Visible absorption time traces for $[Fe^{IV}O(L_5^2)]^{2+}$ at 730 nm (middle) and $[Fe^{III}(OOH)(L_5^2)]^{2+}$ at 537 nm (right) for the reaction of **1** (2 mM) with 50 equiv. H_2O_2 in the presence of various equiv. 2,6-lutidine (indicated by x) in CH_3OH at 20°C.

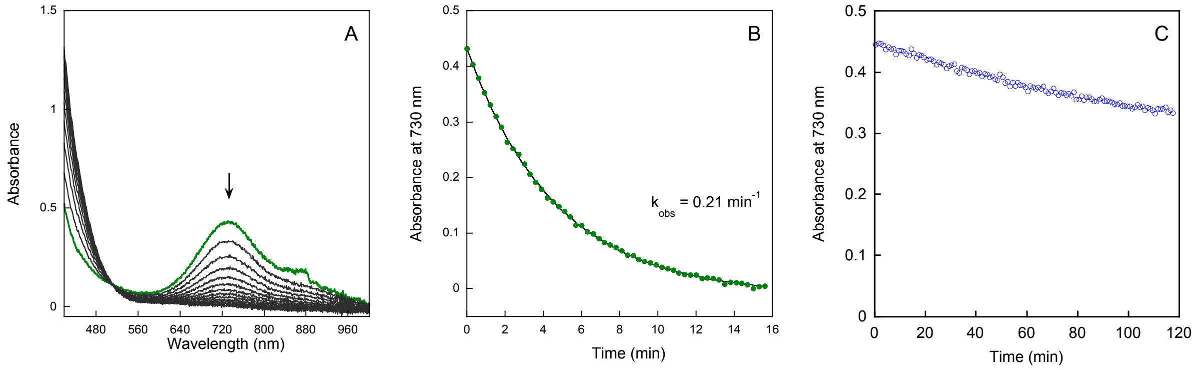

Figure S7. UV-visible (**A**) and time trace at 730 nm (**B**) of $[Fe^{IV}O(L_5^2)]^{2+}$ (1.5 mM in MeCN/MeOH (1/1 v/v) at 20°C; and (**C**) time trace at 730 nm of a similar sample in neat MeCN.

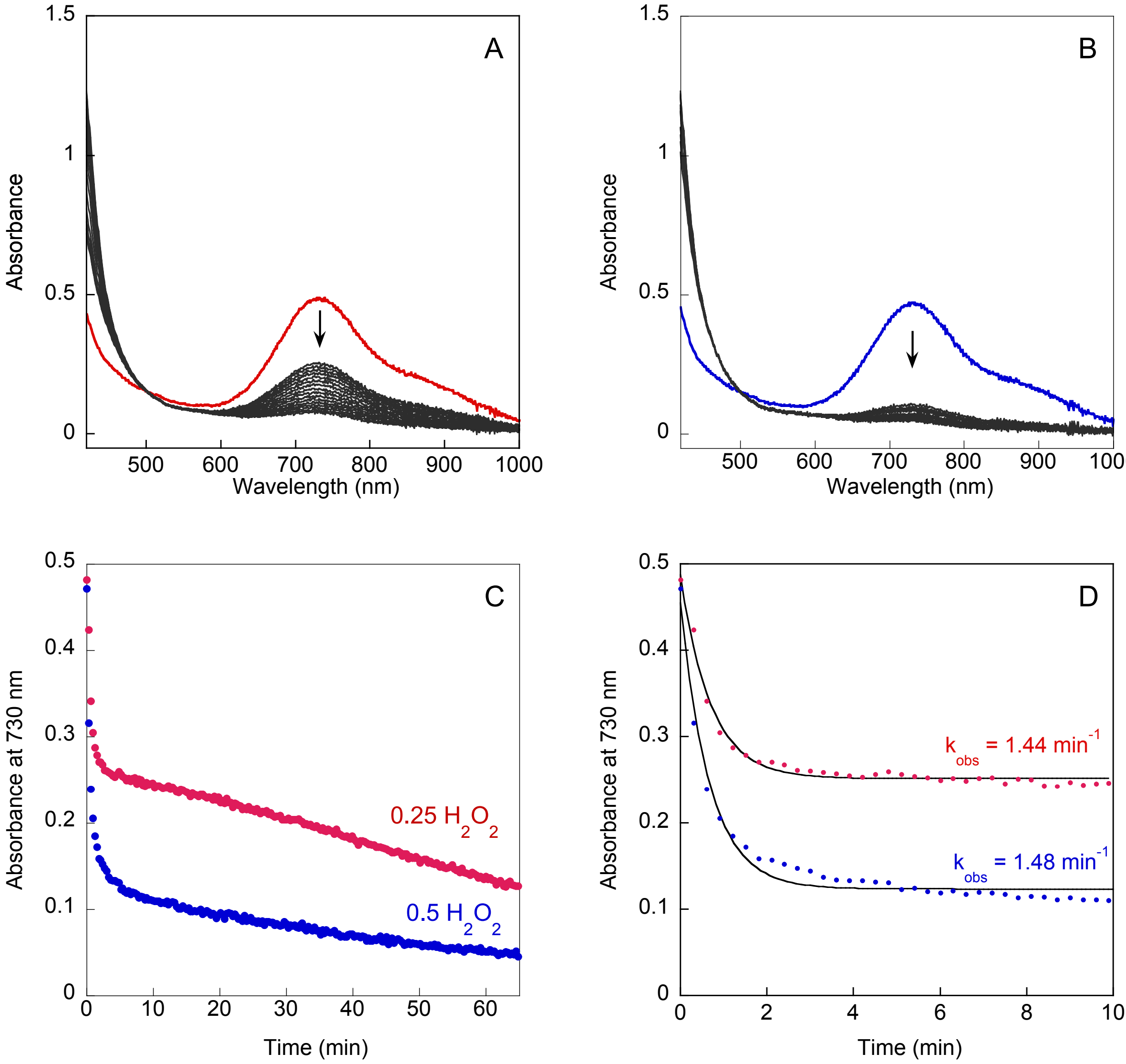

Figure S8. Evolution of the UV-visible spectrum of $[Fe^{IV}O(L_5^{2})]^{2+}$ (1.6 mM in MeCN) at 20°C in the presence of 0.25 equiv. H_2O_2 (**A**) or 0.5 H_2O_2 (**B**), and time traces at 730 nm over 65 minutes (**C**), or focusing on the first 10 minutes (**D**). Red and blue dots correspond to the reaction mixtures containing 0.25 or 0.5 equiv. H_2O_2 .

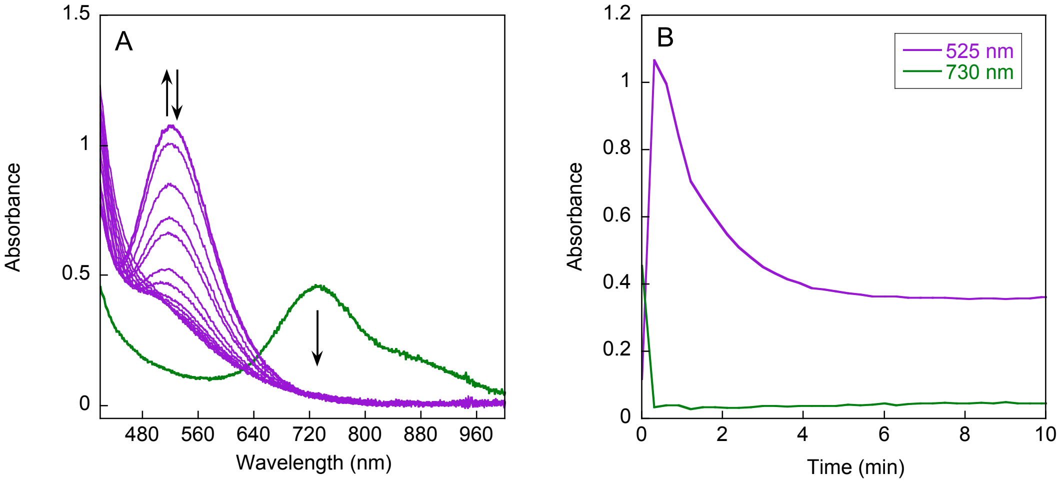

Figure S9. Evolution of the UV-visible spectrum of $[Fe^{IV}O(L_5^2)]^{2+}$ (1.5 mM in MeCN) at 20°C in the presence of 50 equiv. H_2O_2 (**A**) and time traces at 730 (green line) and 525 nm (purple line) (**B**).

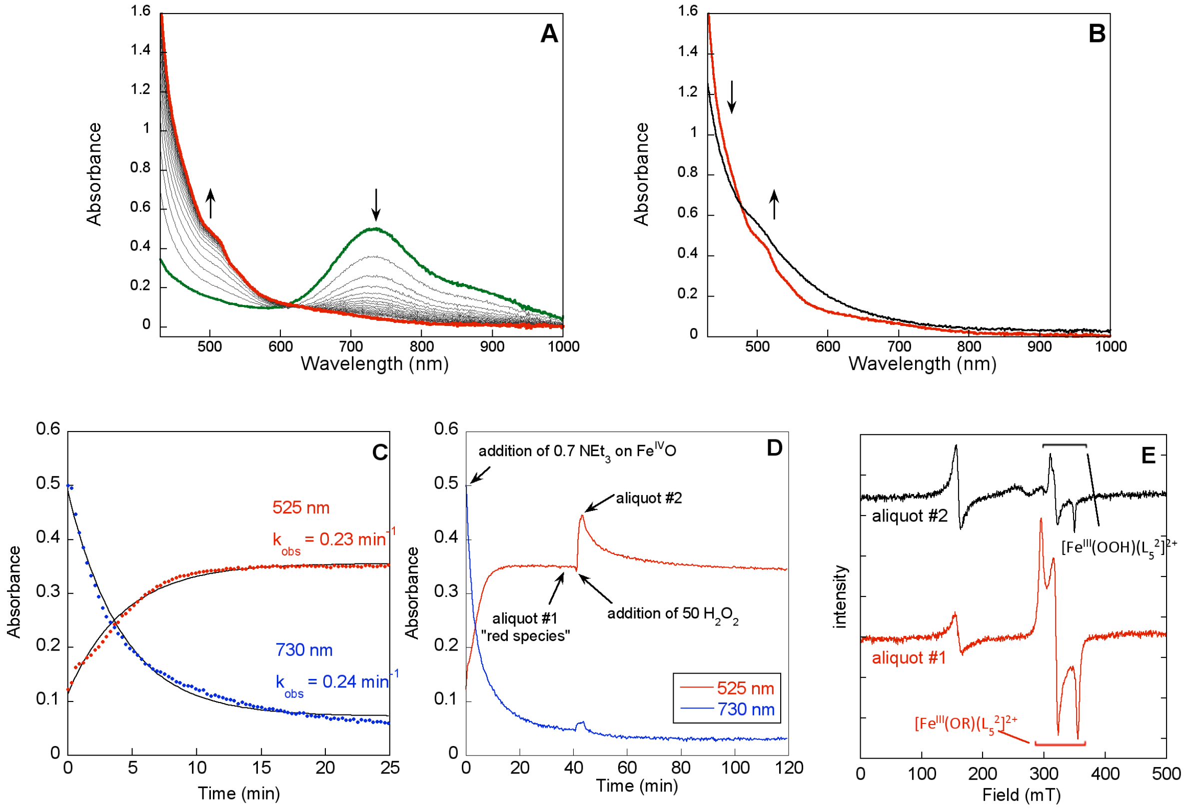

Figure S10. (**A**) Evolution of the UV-visible spectrum of $[Fe^{IV}O(L_5^2)]^{2+}$ (1.6 mM in MeCN) at room temperature in the presence of 0.7 NEt_3 (green) and evolution towards the red species (red). (**B**) Effect of the addition of 50 equiv. H_2O_2 on the red species monitored by UV-visible. (**C**) Time traces at 730 nm and 525 nm for the spectral evolution displayed in panel **A**. (**D**) Time traces at 730 nm and 525 nm upon addition of 50 equiv. H_2O_2. (**E**) EPR spectra for the samples taken before and after addition of H_2O_2 as indicated in panel **D**.

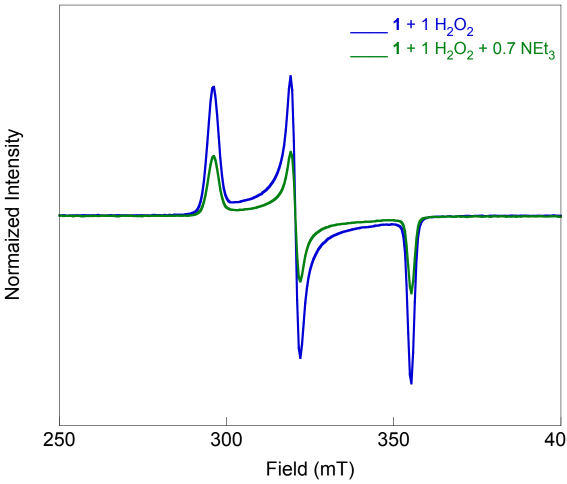

Figure S11. X-band EPR at 90 K of **1** (2 mM) with 1 equiv. H_2O_2 in the presence (green trace) or absence (blue trace) of 0.7 equiv. NEt_3 in CH_3OH at 20°C. Microwave power 1 mW, modulation amplitude 8 G, gain 50 dB. The intensity of these spectra have been normalized and can be directly compared.

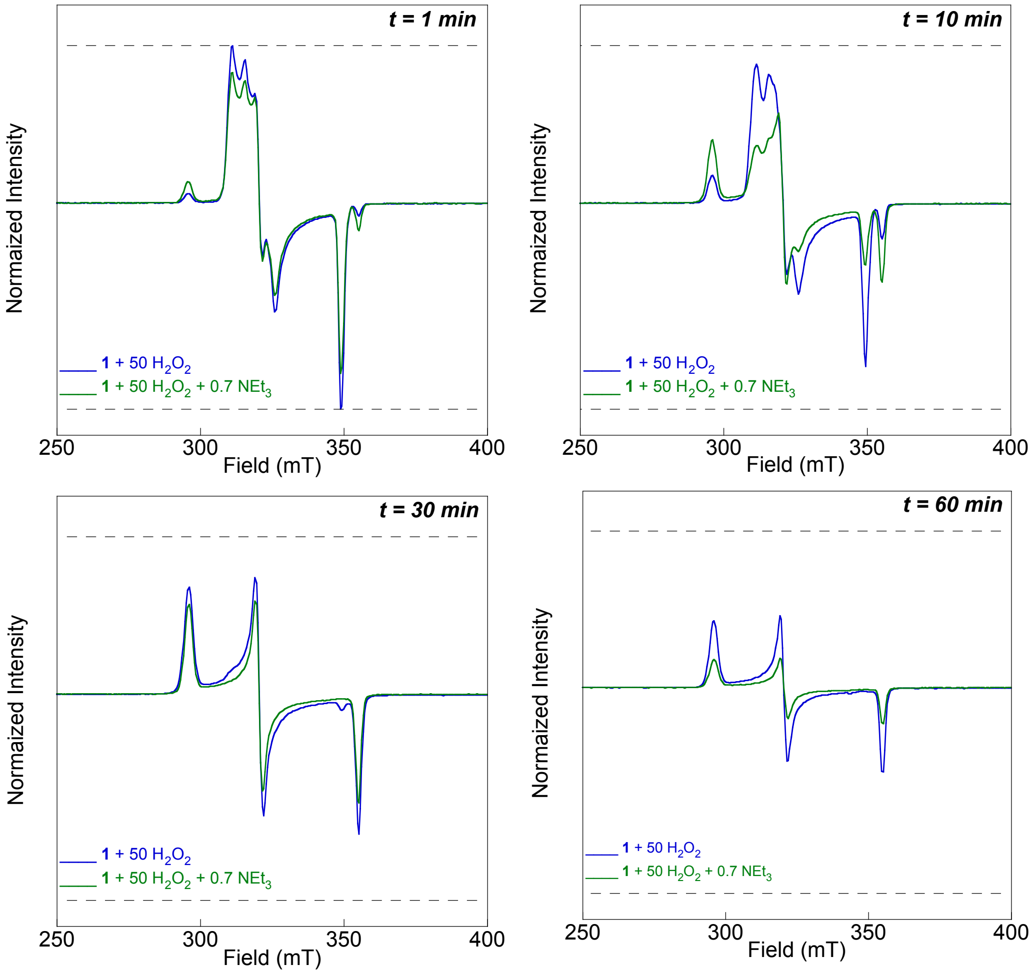

Figure S12. X-band EPR spectra monitored in time for the reaction of **1** (2 mM) with 50 equiv. H_2O_2 in the presence (green trace) or absence (blue trace) of 0.7 equiv. NEt_3 in CH_3OH at 20°C. T = 90 K, microwave power 1 mW, modulation amplitude 8 G, gain 50 dB. The intensity of these spectra have been normalized and can be directly compared.

references.

1 P. Mialane, A. Nivorojkine, G. Pratviel, L. Azéma, M. Slany, F. Godde, A. Simaan, F. Banse, T. Kargar-Grisel, G. Bouchoux, J. Sainton, O. Horner, J. Guilhem, L. Tchertanova, B. Meunier and J.-J. Girerd, *Inorg. Chem.*, 1999, **38**, 1085–1092.

2 A. Thibon, J. England, M. Martinho, V. G. Young Jr, J. R. Frisch, R. Guillot, J.-J. Girerd, E. Münck, L. Que Jr. and F. Banse, *Angew. Chem. Int. Ed.*, 2008, **47**, 7064–7067.

3 G. M. Sheldrick, SHELXS-97, Program for Crystal Structure Solution, University of Göttingen, Göttingen, Germany, **1997**.

4 G. M. Sheldrick, *Acta Crystallogr., A, Found. Crystallogr.*, 2008, **64**, 112–122.

5 L. J. Farrugia, *J Appl Crystallogr*, 1999, **32**, 837–838.